Brain Stimulation 18 (2025) 1705–1717

Contents lists available at ScienceDirect

Brain Stimulation

journal homepage: www.journals.elsevier.com/brain-stimulation

Flexible and stable cycle-by-cycle phase-locked deep brain stimulation system targeting brain oscillations in the management of movement disorders

Xuanjun Guo [a,b,c], Alek Pogosyan [b], Jean Debarros [b], Shenghong He [b], Laura Wehmeyer [b], Fernando Rodriguez Plazas [b], Karen Wendt [b,d], Zixiao Yin [e], Ahmed Raslan [f], Thomas Hart [g], Francesca Morgante [g], Tim Denison [b,d], Erlick A. Pereira [g], Keyoumars Ashkan [f], Shouyan Wang [a,c], Huiling Tan [b,*]

[a] Institute of Science and Technology for Brain-Inspired Intelligence, Fudan University, Shanghai, China
[b] Medical Research Council Brain Network Dynamics Unit, Nuffield Department of Clinical Neurosciences, University of Oxford, Oxford, United Kingdom
[c] MOE Frontiers Center for Brain Science, Fudan University, Shanghai, China
[d] Department of Engineering Science, University of Oxford, Oxford, United Kingdom
[e] Department of Neurosurgery, Beijing Tiantan Hospital, Capital Medical University, Beijing, China
[f] Department of Neurosurgery, King's College Hospital, Denmark Hill, London, United Kingdom
[g] City St George's, University of London & St George's University Hospitals NHS Foundation Trust, Neuroscience & Cell Biology Research Institute, Cranmer Terrace, London, United Kingdom

ARTICLE INFO

Keywords:
Phase-locked stimulation
Kalman filter
Non-resonant oscillators
Parkinson's disease
Closed-loop neuromodulation

ABSTRACT

Background: Precisely timed brain stimulation, such as phase-locked deep brain stimulation (PLDBS), offers a promising approach to modulating dysfunctional neural networks by enhancing or suppressing specific oscillations. However, its clinical application has been hindered by the lack of user-friendly systems and the challenge of real-time phase estimation amid stimulation artifacts.

Material and method: In this work, we developed a clinically translatable PLDBS framework that enables real-time, cycle-by-cycle stimulation using standard amplifiers and a computer-in-the-loop system. Our approach integrates Kalman filter-based artifact suppression and non-resonant oscillators for accurate phase tracking. We tested this system in a small clinical trial ($n = 4$) targeting subthalamic nucleus (STN) stimulation at specific phases of cortical alpha and STN beta rhythms in patients with movement disorders during acute lead externalization following deep brain stimulation surgery.

Result: The system delivered stimulation with over 90% accuracy, within $\pm\pi/2$ for STN beta and $\pm\pi/4$ for cortical alpha. Stimulations delivered at different STN beta phases led to a significant difference in evoked potentials in STN local field potentials in all participants. STN beta-triggered stimulation showed potential phase-dependent modulation of finger-tapping velocity and amplitude in Parkinson's disease.

Conclusion: This study presents a flexible and stable pipeline for precise PLDBS with CE-marked devices and a computer-in-the-loop. Using this pipeline, we showed that PLDBS at different STN beta phases differentially modulates the evoked action potentials in the STN and motor behavior used to quantify bradykinesia, paving the way for further studies and clinical trials for PLDBS.

1. Introduction

Phase-locked neurostimulation [1,2] is an innovative neuromodulation technique that harnesses the principles of synchronizing stimulation and neuronal oscillations to modulate brain activity for therapeutic purposes [3–7]. Phases of a neural oscillation indicate moment-to-moment fluctuations in neuronal excitability [8–10], suggesting that stimulation delivered at specific phases (Fig. 1A) can lead to more precise modulation of neuron population activities and, consequently, more pronounced physiological and behavioral effects [11–20].

* Corresponding author.
E-mail address: huiling.tan@ndcn.ox.ac.uk (H. Tan).

https://doi.org/10.1016/j.brs.2025.09.002
Received 4 May 2025; Received in revised form 21 August 2025; Accepted 5 September 2025
Available online 6 September 2025

Targeting particular phases of neural oscillations with different stimulation modes, including transcranial magnetic stimulation [21], transcranial electrical stimulation [16,22,23], deep brain stimulation (DBS) [2,24,25], and acoustic stimulation [26,27], has shown potential in influencing neuronal rhythms and improving cognition [5,28,29], movement [30] and sleep [22,26,27]. These approaches show promise for therapeutic applications in disorders such as essential tremor [13,31], Parkinson's disease (PD) [32,33], and depression [34,35], by precisely modulating brain network dynamics, which can subsequently influence behavior. While preclinical studies in movement disorders have indicated the efficacy of phase-targeted neuromodulation in bidirectionally regulating oscillatory dynamics (particularly subthalamic nucleus (STN) beta oscillations [32,33]) to potentially modify motor outcomes [36], critical gaps persist in translating these electrophysiological interventions into clinically viable behavioral modulation paradigms.

Achieving effective phase-locked neurostimulation requires overcoming two interdependent technical barriers: robust elimination of stimulation artifacts that obscure endogenous neural oscillations during stimulation and precise tracking of instantaneous phase dynamics [37]. Various methods have been proposed for artifact mitigation including bandpass filter [38–40], template subtraction [24,25,41], and blanking combined with interpolation [32,42–44]. In parallel, techniques such as phase inversion detection [45,46], phase-locked oscillators [14,47], analytic signal construction [23,48,49], state-space model [32,50,51] and resonant theory [52] have been employed for real-time phase estimation. Despite these advances, cycle-by-cycle phase-locked DBS (PLDBS) targeting neural signals near stimulation sites still faces challenges [53]. Specifically, stable device-independent artifact removal methods remain elusive, and optimal approaches for accurate phase estimation in the presence of residual artifacts have yet to be established.

Here we aim to establish a framework allowing clinical testing of PLDBS, that integrates an effective artifact removal method with an optimized real-time phase estimation algorithm, ensuring reliable continuous cycle-by-cycle phase tracking. To achieve this, we have:1) compared different methods required for real-time phase estimation and artifact suppression in simulation, 2) evaluated different factors contributing to the potential variability in the performance of PLDBS; and 3) demonstrated the feasibility of the proposed method and hardware pipeline for PLDBS in patients and provided pilot data showing phase-specific effect of PLDBS. This pipeline we proposed is compatible with commonly used amplifiers. Using a computer-in-the-loop for real-time signal processing, we evaluated its real-time phase estimation accuracy and stability in cycle-by-cycle PLDBS targeting cortical and subthalamic oscillations in human patients. Moreover, our results suggest that PLDBS at different STN beta phases differentially modulates evoked resonant neural activity (ERNA) in the STN, a modulation-responsive electrophysiological biomarker reflecting basal ganglia-thalamocortical circuit reorganization in PD [54–56], and motor behavior related to bradykinesia, underscoring its potential for clinical application and paving the way for further studies and clinical trials.

2. Material and methods

2.1. Real-time artifact removal method

We first reviewed several stimulation artifact removal methods, including template subtraction, interpolation, and sampling, as described in Supplementary Materials (Supp Table 1).

Template subtraction assumes that the artifacts associated with each stimulation pulse follow a constant pattern. However, this assumption only applies when amplifiers with very high-sampling-rate (e.g. 44k Hz) and large dynamic ranges. In most cases, stimulation artifacts appear as random waveforms [41], making template subtraction ineffective. Beyond that, recently proposed methods such as blanking or irregular sampling [43] and interpolation depend on precisely knowing the stimulation artifact duration. The high-frequency components of square-waved stimulation pulses cause prolonged signal ringing after amplifier anti-aliasing filtering, representing its "impulse" response to

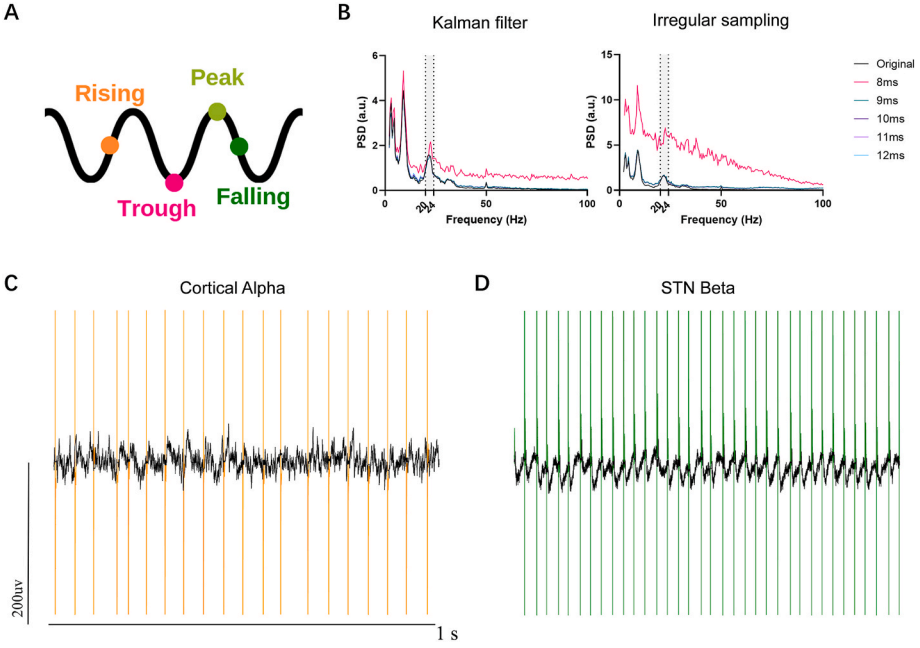

Fig. 1. – Artifacts removal based on Kalman filter in simulation and real-test in participants. (A) Schematic illustration of phase definitions: rising (0°), peak (90°), falling (180°), and trough (– 90°). (B) PSD analysis comparing the original signal with artifact-suppressed signals processed using either the Kalman filter (left) or irregular sampling (right). The analysis was performed across different parameter settings for estimated artifact durations (8 ms, 9 ms, etc.). (C) Representative 2-s cortical alpha-triggered PLDBS signals: processed signal using the Kalman filter (black) overlaid on the raw signal (orange; stimulation delivered at rising phase). (D) Representative 2-s STN beta-triggered PLDBS signals: processed signal using the Kalman filter (black) overlaid on the raw signal (dark green; stimulation delivered at falling phase).

the stimulation pulse. Thus, the type of frontend circuit, the analog-to-digital converter technology, and the digital filtering technique influence the stimulation artifact duration and temporal shape, making removing it extremely challenging to mitigate with standard methods [57].

The Kalman filter [58,59] reduces uncertainty in the estimated signal by combining direct measurements with estimations based on a model, following Bayesian principles. It employs a "blanking" mechanism, where the confidence in the measurements is set low when stimulation artifacts are present. During these periods, the signal estimation is instead driven by a model. This study proposes using the Kalman filter for artifact removal with a second-order autoregressive (AR) model based on past data points. Unlike simpler interpolation techniques that either skip or replace artifacts with preset values, the Kalman filter adapts to variations in the signal, providing a more precise reconstruction of underlying neural activity. We evaluated the performance of the Kalman filter in artifact suppression and compared it against irregular sampling (blanking).

2.2. Real-time phase estimation method

Several methods for phase estimation used in previous studies were considered, including zero-crossing (ZC), phase-locked oscillators, causal Hilbert transform (HT) methods such as endpoint-corrected HT (ecHT) [49] and autoregressive HT (arHT) [15,48,60,61], state space phase estimator (SSPE) [50], resonant oscillators (RO), non-resonant oscillators (NRO) [52,62] and OscillTrack [32], as detailed in supplementary materials (Supp Table 2). Some of these approaches have been compared in previous literature (Supp Fig. 1) [50–52,62]. NRO has been shown to outperform RO, ecHT, and phase-locked oscillators in neural oscillations, offering a broader targeted frequency band. SSPE also outperforms the HT and ZC approaches, showing greater tolerance to noise. However, no study has compared different methods and established a reliable pipeline for PLDBS scenarios, particularly when combined with stimulation artifact removal techniques.

We implemented ZC, arHT, NRO, SSPE, and OscillTrack in our study based on prior research. We compared their performance in a simulation model using real recordings and synthetic signals containing stimulation artifacts. Given that most of these models construct the analytic signal which allows us to extract the instantaneous amplitude and phase (with ZC modified to use a moving window), we additionally evaluated real-time amplitude estimation by computing the mean squared error between the estimated amplitudes and the ground truth (Supp Table 3).

2.3. Simulink model

To identify a stable method for phase estimation under varying signal-to-noise ratios and stimulation artifacts, we implemented and

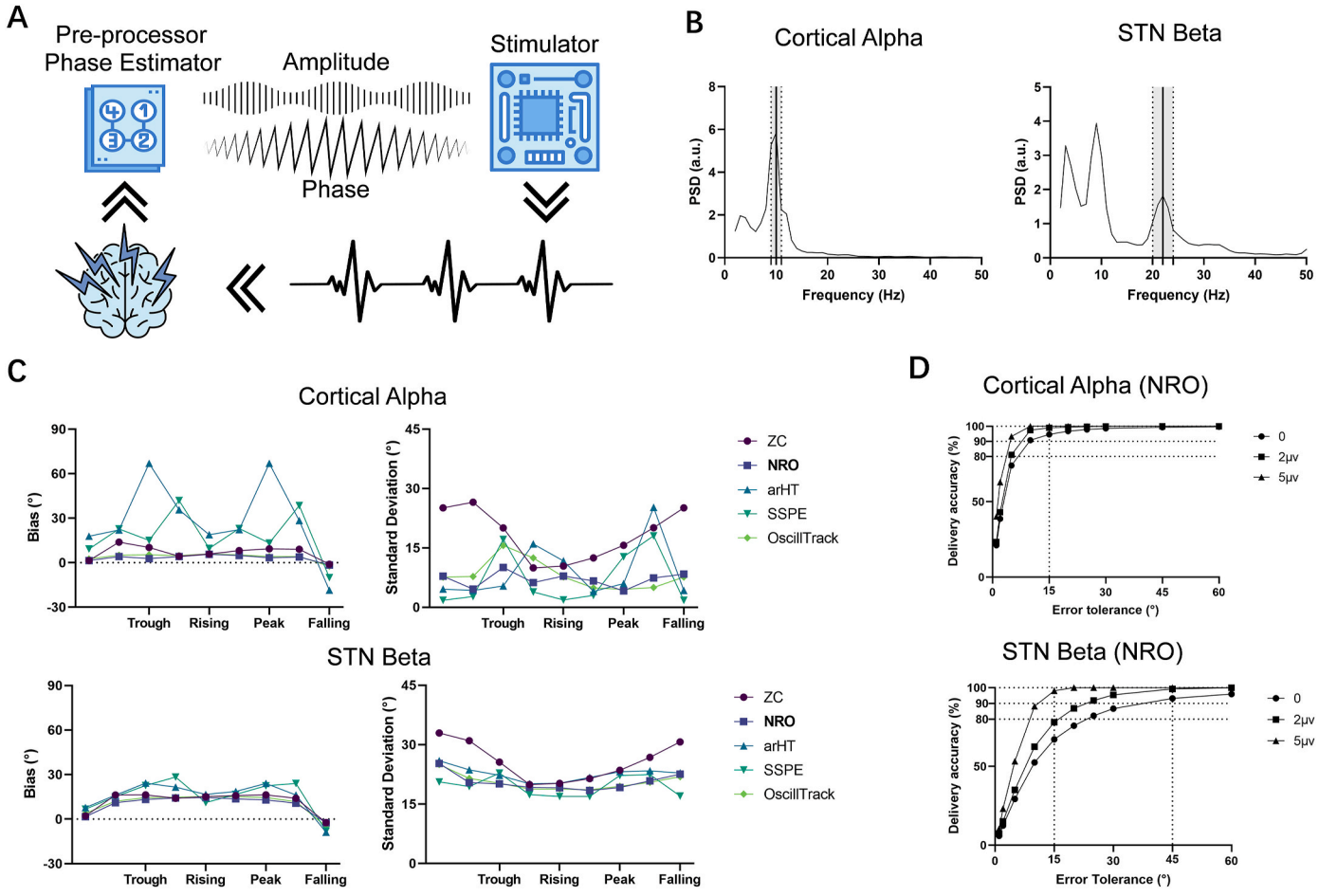

Fig. 2. Performance evaluation of PLDBS using Kalman filtering and NRO analysis. (A) Simulation of real-time PLDBS system. Neural signals undergo three-stage processing: (1) Artifact removal via Kalman filtering with bandpass filtering, (2) Instantaneous phase estimation, and (3) Phase-triggered stimulation delivery. (B) Spectral characteristics of cortical alpha and STN beta oscillations. Peak frequencies (vertical bars) with corresponding filter bandwidths (dashed lines) demonstrate oscillation-specific spectral filtering. (C) Phase estimation performance comparison across five methods. NRO showed superior performance with minimal *bias* and reduced *std*. (D) Stimulation timing accuracy showed precise targeting simulation with cortical alpha and STN beta oscillations.
Abbreviation: PLDBS: phase-locked deep brain stimulation, PSD: power spectral density, STN: subthalamic nucleus, ZC: Zero-crossing, NRO: Non-resonant oscillators, arHT: autoregressive Hilbert Transform, SSPE: state space phase estimator.

tested the different methods using Simulink, a MATLAB-based modeling environment. The designed model incorporates several modules, including data input, artifact removal, preprocessing, phase estimation, and stimulation (adding stimulation artifacts). After initial artifact suppression, the signals undergo fourth-order Chebyshev Type I bandpass filtering to ensure narrow-band frequency isolation. Although the IIR bandpass filter introduces a non-linear phase response across frequency bands (Supp Fig. 2), it maintains an approximately linear phase response within the passband. It preserves most amplitude information, enabling the phase estimation method to retrieve the real-time phase (Supp Fig. 3) effectively. The conditioned signals are then processed through the mentioned phase tracking algorithms to compute instantaneous phase dynamics. Finally, the model triggers phase-locked stimulation, where stimulation pulses are delivered at the target phase, with the stimulation artifacts added to the original input signal (Fig. 2A). The methodological configurations for phase estimation were derived from the previously proposed optimization framework [15,48,60,61].

2.4. Simulation input data and validation

Validation was performed using real recordings. The first dataset comprised 25-s eyes-closed resting-state electroencephalogram (EEG) recordings from the Pz electrode in a healthy participant, with robust cortical alpha oscillations (Fig. 2B, left). The second dataset consisted of 60-s STN LFP recordings from a PD patient during OFF medication and OFF stimulation, exhibiting pathologically elevated beta-band synchrony (Fig. 2B, right), derived from our previously published paper [63]. Both clinical datasets were sampled at 4096 Hz and preprocessed through identical 2 Hz fourth-order Butterworth high-pass filtering. The local ethics committees approved the study, and all patients provided written informed consent according to the Declaration of Helsinki.

For each dataset, the instantaneous phase of the target oscillation was computed offline using the "gold standard" technique (i.e., offline Hilbert transform (oHT)), applied to the raw signal without artifacts. To systematically evaluate the phase-locking performance of different algorithms, we implemented a simulation framework that spanned the entire phase space (−180°–180°, 45° increments). Two key metrics were used for evaluation: *bias* (absolute mean error between real-time delivered phases and offline gold-standard target phases) and the *std* (standard deviation of delivered phases) during each phase-locked stimulation simulation.

$$bias = mean\left|\varphi_{delivery} - \varphi_{predetermined}\right|$$

$$std = std\left(\varphi_{delivery}\right)$$

Further quantification included phase-specific *accuracy*, defined as the proportion of pulses delivered within incremental tolerance thresholds (0°, 2°, 5°, 10°, 15°, 20°, 25°, 30°, 45°, 60°), and calculated as:

$$accuracy = \frac{N_{\left|\varphi_{delivery} - \varphi_{predetermined}\right| < tolerance}}{N_{all}}$$

Since estimation errors may vary with the amplitude of the target oscillation [52], amplitude-dependent gating thresholds of 2 μV and 5 μV were applied to the offline signal. The accuracy of the signal segments above these thresholds was evaluated to determine potential improvements in stimulation *accuracy*.

2.5. PLDBS hardware implementation

Following computational validation, we implemented a closed-loop PLDBS system integrating CE-marked amplifiers (TMSi Saga, TMS International, Netherlands) and CE-marked stimulators (ISIS, Inomed Neurocare Ltd., Germany) with real-time processing via MATLAB and Lab Streaming Layer (Fig. 3A/5A). Signals (4096Hz unipolar sampling) underwent 2 Hz Butterworth high-pass filtering before Kalman filter-based artifact suppression and NRO phase estimation. Once the

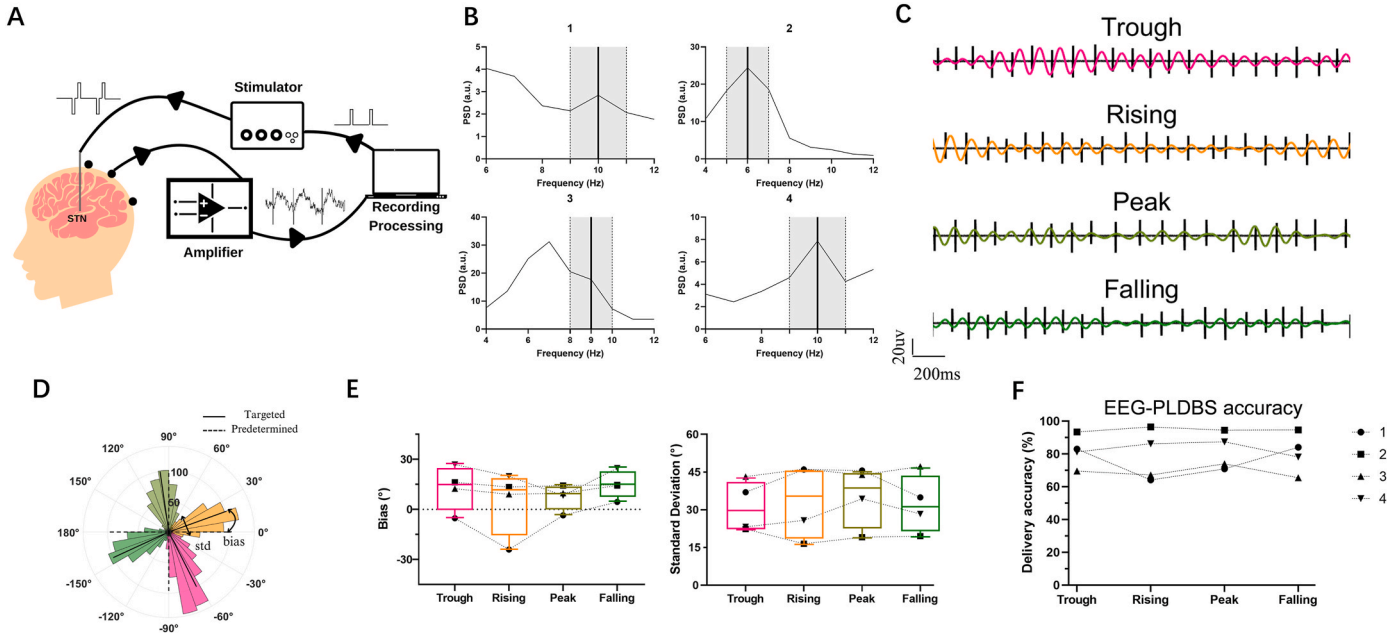

Fig. 3. PLDBS of cortical alpha oscillations. (A) The PLDBS system delivered electrical pulses to the STN based on alpha oscillations recorded from an EEG channel. (B) Individualized spectral profiles of the four patients. Vertical lines denote individualized alpha peak frequency with 3 Hz bandwidth filters (gray shaded area). (C) Phase-locked stimulation exemplar (Participant 4, Oz channel, left hemisphere targeting). Representative 2-s traces show stimulation timing at four quadrant alpha phases: trough (pink), rising (orange), peak (yellow-green), and falling (dark green). Wideband EEG with stimulation artifacts is shown in black. (D) Angular distribution of stimulation phases for Participant 4. Circular histograms show phase concentration at targets (dashed lines) with mean vectors (black lines). (E) Phase estimation consistency across participants. In the figure, each point represents a participant's phase-specific calculated value. A Friedman test revealed a significant phase-dependent effect in *bias* (left), while *std* (right) remained stable across target phases. (F) Targeting accuracy across phase quadrants. Overall system achieved 81.24% ± 3.53% accuracy (±45° tolerance) with comparable performance across phases.

difference between the estimated and target phases drops below a specific threshold (set as 2°), a trigger signal is sent to the neurostimulator via Labjack. This brief TTL pulse trigger signal enables the stimulator to deliver a single stimulation pulse.

Artifact detection is triggered at a 300 μV threshold. Based on previously recorded data [63] and analysis results (Fig. 1B–Table 2), the Kalman filter estimates LFPs during the subsequent 9 ms. For real-time phase estimation, the NRO method, which outperformed others in simulations, was implemented. This method uses a linear oscillator model $\ddot{x} + \alpha\dot{x} + \omega^2 x = s(t_k)$, solved numerically to map the analytic input signal's oscillator dynamics (amplitude/phase). We set $\alpha_{amplitude} = 80$, $\alpha_{phase} = 10$ following the methodology in Ref. [64], where $\alpha_{amplitude}$ and α_{phase} are the damping parameters for amplitude and phase estimation, respectively. A large $\alpha_{amplitude}$ ensures stable amplitude tracking by providing strong damping, while a smaller α_{phase} minimizes phase distortion. The oscillator frequency was set to $\omega = 5\vartheta$, with $\vartheta = 2\pi \cdot f_{peak}$, where f_{peak} is the target oscillation frequency.

2.6. PLDBS test in human patients

The PLDBS system was tested in four patients (Table 1), including one with cervical dystonia and three with PD, all undergoing STN targeted DBS surgery. The implanted DBS systems were from two manufacturers: Medtronic Inc. (USA) with octopolar directional leads (SenSight™ model 33005), and Boston Scientific (USA) with octopolar directional leads (Vercise™ model DB-2202). Electrodes were connected to temporary lead extensions and externalized through the temporal or frontal scalp. Recordings were performed in the OFF-dopaminergic medication state, four to six days postoperatively. Monopolar stimulation was applied using an ISIS neurostimulator, with a self-adhesive electrode placed on the participant's back as the reference. Stimulation was triggered only when the signal amplitude, as estimated by the amplitude estimator, exceeded 0.5 μV, ensuring that activation occurred under physiologically meaningful conditions. The stimuli consisted of symmetric, constant-current, biphasic pulses (3 mA, 60 μs, with the negative phase delivered first). The local ethics committees approved the study, and all patients provided written informed consent according to the Declaration of Helsinki.

Patients remained in a resting seated state throughout the entire recording session. Pre-experimental contact optimization involved 25-pulse mapping (4 mA, 1–0.5 Hz) across STN channels, selecting contacts that elicited maximal ERNA amplitudes in adjacent recordings. A 10-s calibration block was used to quantify fixed system delay (median value of time intervals between trigger onset and stimulation artifact appearance in LFP traces) and temporal jitter (the range of delay measurements across all pulses), which remained constant through all experiments. Multimodal recordings (STN-LFP and EEG, bilateral fingertip accelerometry) were synchronized throughout phase-locked protocols.

Table 1
Clinical information.

	Gender	Diagnose	Handedness	DBS system	Cortical Alpha	STN beta
1	Male	CD	Left	Boston	10Hz	25Hz
2	Male	PD	Left	Medtronic	6Hz	15Hz
3	Female	PD(Tremor)	Right	Medtronic	9Hz	18Hz
4	Male	PD (Bradykinesia)	Right	Medtronic	10Hz	19Hz

Note: Participant 2 exhibited dominant 6Hz theta activity during eyes-closed across all EEG channels, prompting theta-band (6 ± 1.5Hz) PLDBS implementation; Participant 3 demonstrated prominent 7 Hz resting tremor with bi-frequency alpha peaks (7Hz/9Hz), requiring selective 9 Hz alpha targeting. Participants' gender information was collected through a baseline questionnaire, which was completed face-to-face by a trained research assistant at enrollment. Gender options included male, female and other. Abbreviation: CD: Cervical dystonia, PD: Parkinson's disease, DBS: Deep brain stimulation, STN: Subthalamic nucleus.

Table 2
Kalman filter outperforms irregular sampling with matched parameters.

Estimated artifacts durations/ms	8	9	10	11	12
Irregular sampling	409.91 %	14.56 %	13.52 %	11.41 %	10.84 %
Kalman filter	**36.18 %**	**5.21 %**	**5.56 %**	**5.62 %**	**5.84 %**

2.7. Cortical alpha-triggered PLDBS

Alpha oscillations are commonly observed in the parietal lobes via EEG recordings, especially with eyes closed, and are associated with rhythmic fluctuations in excitability [65,66]. To validate the PLDBS efficacy, we implemented cortical alpha-triggered PLDBS as a proof-of-concept demonstration (Fig. 3A). Before stimulation, participants were asked to close their eyes while feedback channels exhibiting the highest alpha-band spectral power were selected from standard EEG (Fz, Cz, Pz, Oz). Individualized alpha peak frequencies were identified using power spectra density (PSD) analysis and extracted with 3 Hz bandwidth filters centered on the dominant frequency (Fig. 3B). The cortical alpha-triggered PLDBS protocol targeted four cardinal phase points: rising (0°), peak (90°), falling (180°), and trough (−90°) see as Fig. 1A. Each phase condition was tested in duplicate 30-s stimulation trials (8 total blocks) administered in a randomized sequence, with 60-s inter-block washout intervals.

2.8. STN beta-triggered PLDBS

Beta oscillations in STN have been associated with bradykinesia and rigidity in PD, and STN beta-triggered PLDBS may more effectively modulate these pathological rhythms [67–69]. We implemented STN beta-triggered PLDBS in four participants (Fig. 5A). The feedback channel was selected based on the contact exhibiting the highest ERNA amplitude during contact optimization. Participant-specific beta peak frequencies were derived from resting-state PSD analyses (OFF stimulation) and extracted using a 5 Hz bandwidth filter (Fig. 5B). Consistent with prior studies [36,70], STN beta-triggered PLDBS targeted two antithetical oscillation phases: rising (0° or 20°) and falling (180° or −160°). Each phase condition underwent triplicate 30-s stimulation trials (6 total blocks), administered in a randomized sequence, with 60-s inter-block washout intervals. Because the dual-phase paradigm is constrained by system latency parameters (~10 ms jitter), corresponding to 30–50 % of beta-cycle durations (18–30Hz, 33–55 ms/cycle), achieving higher phase resolution within the beta band was not feasible.

2.9. In-vivo validation

Post hoc signal processing employed the same Kalman filter for artifact removal and used oHT as the golden standard to assess PLDBS targeting precision. Performance was evaluated using the same metrics as in simulations: *bias* and *std*. Phase-specific *accuracy* was quantified in two ways: per-target-phase participant means and population-level cross-participant averages. Different phase-locking tolerances were applied based on the oscillation type (cortical alpha-triggered-PLDBS: ±45°; STN beta-triggered PLDBS: ±90°). Consistent with the simulation approach, amplitude-gating thresholds were used to assess the effect of signal amplitude on *accuracy*.

2.10. ERNA modulation with PLDBS

Stimulation phases may bidirectionally modulate beta oscillation amplitudes [32,33,71], but whether these effects relate to stimulation

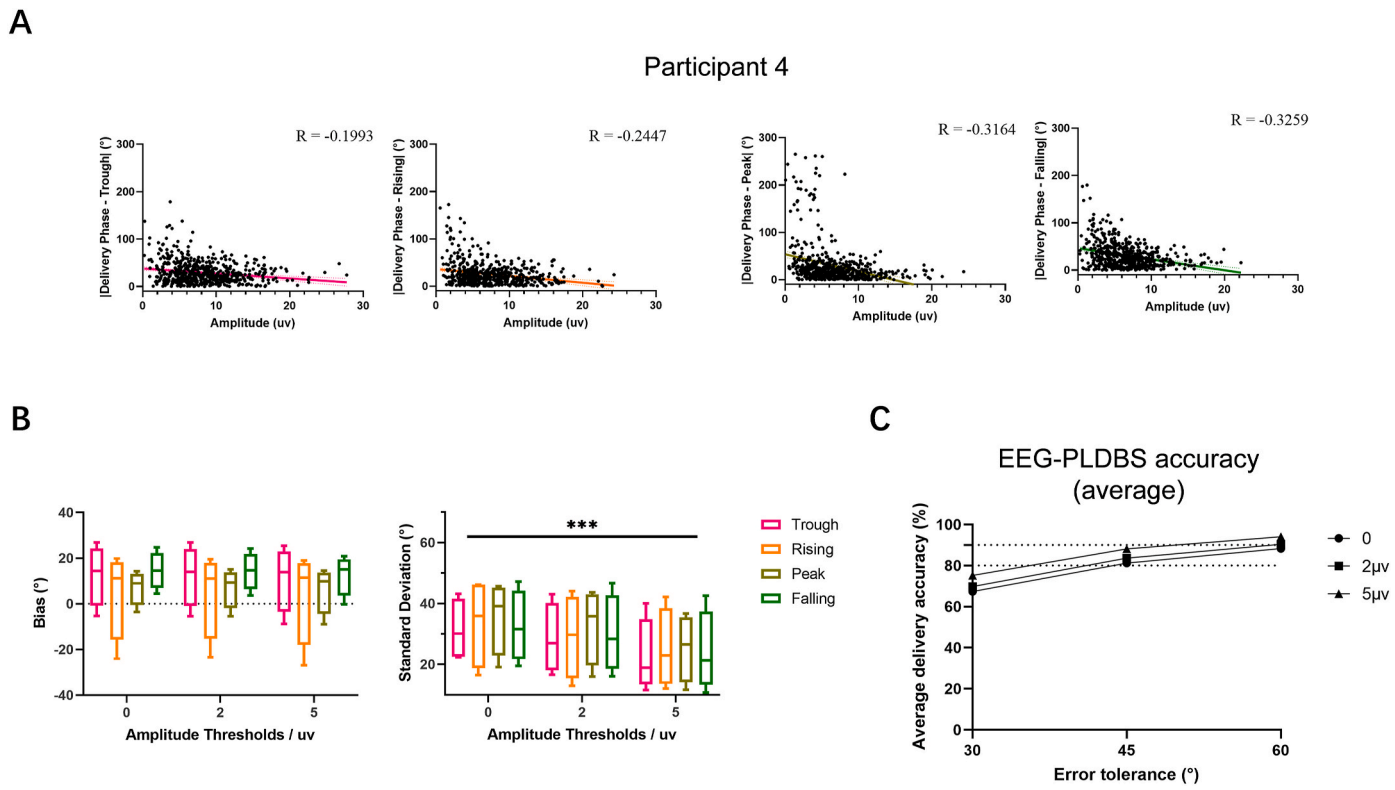

Fig. 4. Amplitude-dependent phase targeting optimization. (A) Phase estimation/targeting error reduced with the increase of instantons amplitude of the target oscillation (cortical alpha) for all the four target phases for Participant 4. Each data point represents a single stimulation pulse, with its phase error and the corresponding amplitude at triggering time. Pearson correlation analysis was performed to assess this relationship on a per-patient basis. A similar negative correlation pattern was consistently observed across all participants. (B) Thresholding efficacy analysis. *Bias* remained consistent when applying amplitude-dependent gating thresholds of 2 μV and 5 μV, while *std* significantly decreased with higher thresholds, independent of stimulation phase. (C) System-wide accuracy improvement. Amplitude gating (5 μV threshold) enhanced phase-locking precision from 81.24% to 88.13% ($\pm 45^{\circ}$ tolerance). (***: $P < 0.001$).

artifacts remains unresolved. Thus, we investigated phase-dependent modulation of ERNA (a candidate electrophysiological biomarker for neuromodulation treatment efficacy, mechanistically linked to STN neuronal firing dynamics [54]) and implemented a standardized feature extraction pipeline based on established frameworks [56,72]. ERNA waveforms were quantified using a custom MATLAB algorithm implementing multiscale peak detection. Signals containing less than two definable peak-trough pairs were excluded via automated quality control. ERNA amplitude was quantified as the absolute difference between the first positive peak and subsequent negative trough. Per-block ERNA amplitudes were calculated as the mean of valid pulse responses occurring within $\pm 45^{\circ}$ and $\pm 90^{\circ}$ tolerance in cortical alpha-triggered PLDBS and $\pm 90^{\circ}$ tolerance in STN beta-triggered PLDBS.

2.11. Finger-tapping task with STN beta-triggered PLDBS

Participant 4, who showed predominant bradykinesia and rigidity, completed a finger-tapping protocol to assess the potential motor modulation effects of PLDBS. As an active control, 130Hz continuous DBS (cDBS) was applied first in two 15-s trials, with OFF recordings before and after serving as baselines (Fig. 7A, top). The PLDBS protocol consisted of two OFF-control blocks and six phase-locked stimulation blocks (Fig. 7A, bottom), each separated by a 3-min washout. Control blocks included pre- and post-15-s trials, while stimulation blocks delivered 60-s trains followed by 15-s finger-tapping under active PLDBS. Phase targeting alternated rising and falling oscillation phases (3 trials each) in a randomized order. The kinematic analysis focused on the axis of maximal acceleration amplitude, considering only accelerometer-discernible tapping peaks. Velocity was derived from the reciprocal inter-peak intervals ($1/\Delta t$), while tapping amplitude was quantified by peak-to-peak accelerometric magnitude.

2.12. Statistics

A few statistical tests have been used to evaluate the potential factors contributing to the variability of the error of real-time phase estimation and PLDBS: (1) Cortical alpha-phase analysis: A Friedman test was employed to compare phase accuracy (*bias* and *std*) across four cortical alpha phases—peak, trough, rising, and falling. This is to evaluate whether the phase estimation accuracy is dependent on the actual target phase. Here, each observation is the average *bias* or the *std* of each target phase for each participant. (2) STN beta-phase performance: A Wilcoxon signed-rank test was used to compare *bias* and *std* between the rising vs. falling phases. Due to the small sample size ($n = 4$), the exact test was performed without normal approximation. Each participant contributed one observation per phase. (3) Stimulation error-amplitude correlations: Pearson correlation analysis was performed to assess whether the error of the phase-estimation correlate with the corresponding amplitude of the target oscillation, on a per-participant basis. In these tests, each observation is each individual target phase detection (or the error of each stimulation pulse). The Pearson correlation coefficient (R value) was reported to quantify the strength and direction of the correlation. (4) Amplitude-gating efficacy: A mixed-effects model was applied to evaluate the influence of the target phase and amplitude threshold on stimulation performance (*bias* and *std*). Linear mixed-effects models were fitted using maximum likelihood estimation. For *bias* and *std*, fixed effects included stimulus phase, amplitude threshold, and their interaction term. Random intercepts for subjects were incorporated to account for repeated measurements. Each participant contributed one *bias* and *std* for each phase-threshold pairing, resulting in 12 observations per

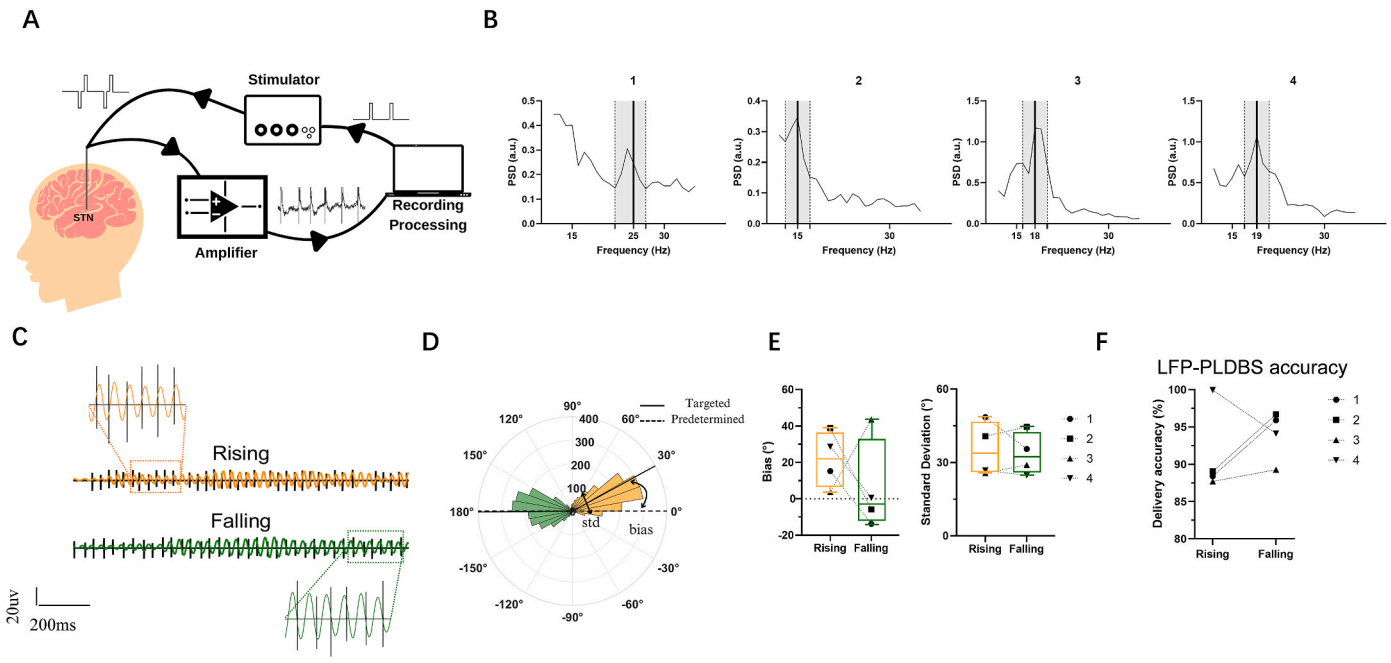

Fig. 5. PLDBS of STN beta oscillations. (A) Based on beta oscillations, the PLDBS system uses an LFP channel to deliver electrical pulses to the STN. (B) Individualized beta spectral profiles. Vertical lines indicate patient-specific beta peak frequencies with 5 Hz bandwidth filters (gray-shaded areas). (C) Phase-locked stimulation exemplars (Participant 4). Representative 2-s traces demonstrate quadrant-specific timing at rising (orange) and falling (dark green) phases. Raw LFP with stimulation artifacts are shown in black (left STN). (D) Angular targeting precision. Circular distributions show phase concentration (dashed lines) at rising and falling with mean resultant vectors (black lines) for Participant 4. (E) Cross-participant phase consistency. *Bias* and *std* did not differ significantly between the two target phases (Wilcoxon signed-rank test). Each participant contributed one observation per phase. (F) LFP-triggered PLDBS demonstrated precise phase-targeting across participants within a ±90° tolerance.

participant (4 phases × 3 thresholds) in EEG-triggered PLDBS and 6 observations per participant (2 phases × 3 thresholds) in LFP-triggered PLDBS. Statistical tests have also been used to test the effect of PLDBS: (5) Stimulation induced ERNA amplitude: One-way ANOVA (for cortical alpha with 4 target phases) or unpaired *t*-test (for STN beta with 2 target phases) were used to evaluate whether stimulation delivered at different phases modulate the ERNA amplitude. These tests were performed for each participant separately, which was motivated by well-documented inter-subject variability in phase-dependent neural responses [68, 73–76]. In these tests, one observation was the ENRA amplitude of each stimulation pulse. To control for inflated statistical power due to the large sample size (as each ERNA following a stimulation pulse was treated as one sample), further testing was performed by applying the same One-way ANOVA or unpaired *t*-test on randomly selected sub-samples (100 trials per condition). This was repeated 1000 times for each participant, the mean and standard deviation of the p-values were reported. (6) Movement modulation: Unpaired t-tests were used to compare finger-tapping performance between cDBS ON and OFF conditions. For PLDBS, a one-way ANOVA with post-hoc comparisons and a correction of the corresponding p-values for multiple comparisons was performed to evaluate differences across rising, falling, and OFF stimulation phases. To optimize statistical power given the limited sample size, we analyzed all valid tapping events as independent observations. Unpaired t-tests were employed because individual trials were not temporally matched across experimental conditions, precluding paired analysis. Trials with missing responses or artifacts were excluded prior to analysis.

All analyses were conducted using custom MATLAB scripts. Correlations are reported as Pearson's R (95 % confidence interval), and all data are presented as *mean* ± *SD*. Post hoc multiple comparisons were conducted using Tukey's HSD procedure with a family-wise error rate controlled at $\alpha = 0.05$.

3. Results

3.1. Kalman filter outperforms irregular sampling in reducing stimulation induced artifacts in the neural recordings

The Kalman filter effectively reduced stimulation artifacts in both simulated and real-time testing scenarios. In simulations with matched parameters for estimated artifact durations, the Kalman filter demonstrated superior performance compared to irregular sampling methods, particularly when the artifact duration was underestimated (Fig. 1B). Specifically, when analyzing beta-band amplitude, the Kalman filter with a predefined 9 ms artifact duration achieved 94.79% artifact suppression (relative error = 5.21%), consistently outperforming irregular sampling (Table 2). Furthermore, real-time implementation confirmed that the Kalman filter developed in this study effectively mitigates stimulation artifacts (Fig. 1 CD), demonstrating its utility in enhancing signal quality for real-time phase estimation.

3.2. NRO following Kalman filter artifact removal provide stable performance for real-time phase estimation

Fig. 2A illustrates the PLDBS simulation pipeline using real recordings, where recorded neural signals were processed in real-time for oscillation phase/amplitude estimation, followed by phase-triggered stimulation. Comparative analysis of estimation *bias* across different methods against oHT identified NRO and OscillTrack as the most accurate (Fig. 2C (left), Table 3). For stability metrics (Fig. 2C (right), Table 3), NRO and SSPE demonstrated superior artifact robustness, exhibiting lower *std*. In addition, both NRO and OscillTrack demonstrated good performance in amplitude estimation (Supp Table 3). Given its optimal phase-tracking precision and robustness to artifacts, NRO was selected as the final phase/amplitude estimation method for the PLDBS implementation.

Stimulation *accuracy* in PLDBS using the Kalman filter and NRO was

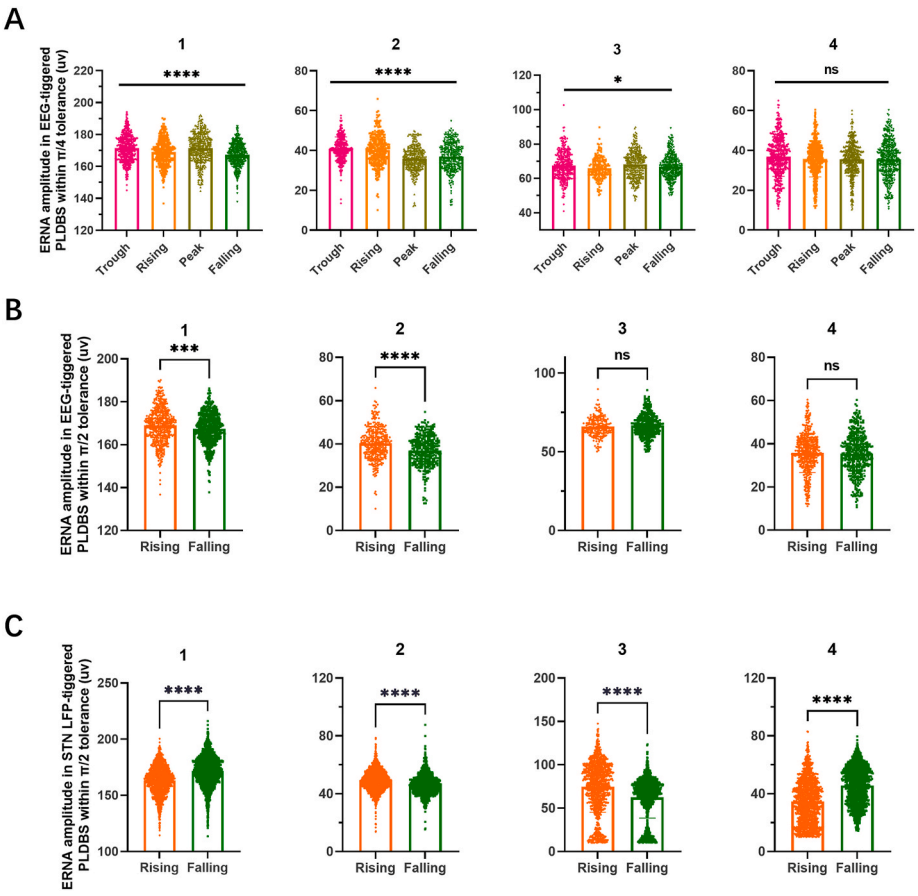

Fig. 6. Differential effect of stimulation phase on ERNA amplitudes. (A) Cortical alpha-triggered PLDBS (±45° tolerance) elicited significant phase-dependent modulation of ERNA amplitudes across four phase windows in Participants 1, 2, and 3, but not in Participant 4. (B) When comparing cortical alpha-phase windows (rising vs. falling, ±90° tolerance), Participants 1 and 2 exhibited significant differences, while Participants 3 and 4 showed no modulation. (C) Significant STN beta-phase-dependent modulation emerged in all participants. (*: $P < 0.05$, *** : $P < 0.001$, **** : $P < 0.0001$).

evaluated next. For cortical alpha oscillations, stimulation *accuracy* reached 94.63% within a ±15° tolerance((Fig. 1D). Similarly, for STN beta oscillations, *accuracy* was 93.24% within a ±45° tolerance (Fig. 1D). Notably, when the amplitude of the target oscillation exceed 2 μV, STN-beta-triggered PLDBS achieved an even higher *accuracy* of 95.42% within a ±30° tolerance.

3.3. Real-time EEG-triggered PLDBS for precise alpha phase targeting

Following a bench test using constant 20 Hz oscillations to validate the system, we conducted cortical alpha-triggered PLDBS in a clinical experiment (Fig. 3A). All participants exhibited strong alpha peaks in EEG recordings (Fig. 3B). Comparisons with oHT analyses confirmed accurate phase targeting across all participants (Fig. 3CD, Supp Fig. 4). The performance of phase estimation and PLDBS remained stable across all target phases (Fig. 3E), as evidenced by a lack of effect of the target-phase on the *bias* ($P = 0.0628, \chi^2(3) = 8.1$, *Kendall's* $W = 0.675$) or the *std* ($P = 0.9004, \chi^2(3) = 0.9$, *Kendall's* $W = 0.075$) with none of the tests survived correction for multiple comparisons. The overall stimulation accuracy across all participants was 81.24% ± 3.53% (Fig. 3F) with ± 45° tolerance: rising: 78.47% ± 15.48%, peak: 81.66% ± 11.14%, falling: 80.56% ± 12.18%, trough: 81.77% ± 9.78%.

PLDBS accuracy was primarily constrained by system latency (hardware/software jitter plus delay) and oscillation amplitude. Trigger precompensation with pre-triggering signals mitigated fixed 25-ms delays, while residual ~10-ms jitter limited phase resolution to 4-phase (alpha) and 2-phase (beta) distinctions. Phase estimation errors were significantly correlated with oscillation amplitude across all target phases and participants (Fig. 4A, an example from Participant 4, Trough: $P < 0.0001, R = -0.1993$, Rising: $P < 0.0001, R = -0.2447$, peak: $P < 0.0001, R = -0.3164$, Falling: $P < 0.0001, R = -0.3259$; Supp Fig. 7). Applying amplitude-dependent gating thresholds of 2 μV and 5 μV to the offline signal resulted in minimal changes in *bias* but a notable reduction in *std* (Fig. 4B). The boxplots illustrate the effects of amplitude threshold (0, 2 and5 μV) on response *bias* and *std* across four stimulation phases: Trough, Rising, Peak, and Falling. For *bias*, a linear mixed-effects model revealed no significant main effect of threshold ($\beta = -0.38, SE = 0.72$, $t(40) = -0.53$, $P = 0.597$) and no significant phase × threshold interaction (all $P > 0.83$), indicating that changes in threshold did not systematically influence directional bias across phases. For *std*, the model revealed a significant main effect of amplitude threshold ($\beta = -1.72, SE = 0.47, t(40) = -3.65, P < 0.001$), with higher thresholds generally associated with lower phase delivery variability. No significant phase × threshold interaction was observed (all $P > 0.5$), suggesting that the variability-reducing effect of higher thresholds was consistent across all stimulation phases. With an amplitude threshold of 5 μV, the average stimulation accuracy within a ±45° tolerance across the four targeted phases improved from 81.24% to 88.13% (Fig. 4C).

3.4. Real-time STN LFP-triggered PLDBS for precise beta phase targeting

To further explore the clinical potential of the PLDBS system, we conducted experiments using STN beta-triggered PLDBS (Fig. 5A). Most stimulation pulses were successfully delivered at the intended target phases (Fig. 5CD, Supp Fig. 5). Phase estimation *bias* ($P = 0.625, W = -4.0$, *median difference* $= -28.53$) and *std* ($P > 0.999$, $W = 0.0$,

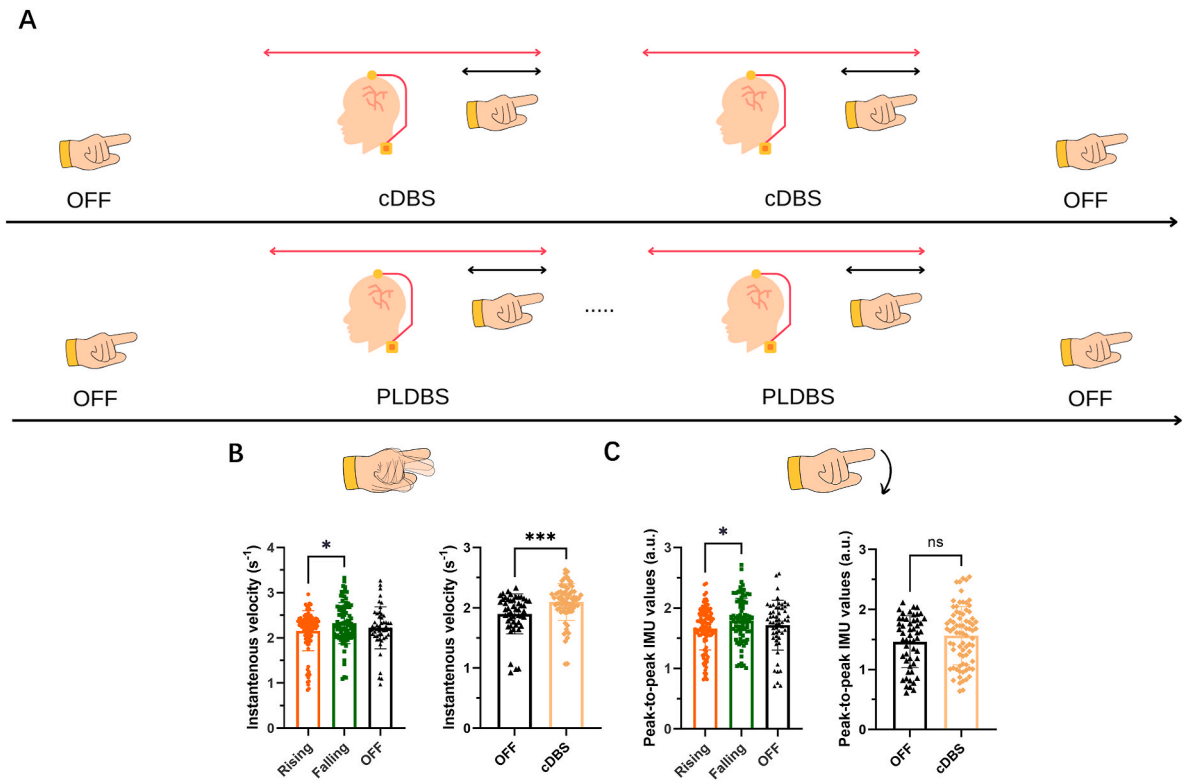

Fig. 7. Differential effect of stimulation phase on finger-tapping task performance. (A) Experimental paradigms for cDBS (top) and PLDBS (bottom) protocols with finger-tapping tasks. For both paradigms, each block included a 60-s stimulation period (red arrows) followed by a 15-s finger-tapping task (black arrows). In the PLDBS protocol, stimulation pulses were phase-locked to the rising and falling phases of beta oscillations, each for three trials, with phase-targeting order pseudorandomized across trials. Two OFF-stimulation control blocks (pre- and post-intervention) were included to assess baseline effects. (B) Finger-tapping velocity was measured for each valid tap. A total of 106, 90, and 55 trials/taps were included in the analysis for the rising, falling, and OFF conditions, respectively. Velocity differed significantly between the rising and falling phases during PLDBS. Additionally, cDBS resulted in significantly higher tapping velocity compared to the OFF-stimulation condition, based on 77 and 53 trials, respectively. (C) Finger-tapping amplitudes (analyzed per valid tap) exhibited phase-dependent differences during PLDBS, whereas only a non-significant trend was observed between OFF and cDBS conditions. (*: $P < 0.05$, *** : $P < 0.001$).

median difference = 0.6459) remained stable across the two target phases (Fig. 5E). The delivery accuracy reaches 92.64% ± 1.753% (Fig. 5F)with ±90° tolerance. Similarly to cortical alpha-triggered PLDBS, estimation error in STN beta-triggered PLDBS significantly correlated with target oscillation amplitude at each phase (an example from Participant 4, rising: $P < 0.0001$, $R = -0.1483$, falling: $P = 0.0009$, $R = -0.07218$; Supp Fig. 8). The weak correlation coefficients suggest stable phase targeting across phases. When applying amplitude-dependent gating thresholds of 2 μV and 5 μV, a linear mixed-effects model revealed that *bias* was not significantly influenced by amplitude threshold ($\beta = -0.39, SE = 6.50, t(20) = -0.06, P = 0.952$) and no interaction was found ($\beta = 0.42, SE = 9.20, t(20) = 0.05, P = 0.964$). For *std*, the model showed a significant main effect of amplitude threshold ($\beta = -0.97$, $SE = 0.46$, $t(20) = -2.12$, $P = 0.046$), with higher thresholds associated with reduced variability. There was no significant phase × threshold interaction ($\beta = 0.651, SE = 0.644, t(20) = 1.01, P = 0.324$), indicating that the thresholding effect was robust across phases.

3.5. Differential effect of stimulation phase on ERNA

The amplitude of the stimulation-induced ERNA in the STN may indicate the cortico-basal ganglia circuit state [55] and reflect DBS-mediated engagement of the basal ganglia indirect pathway [54]. Therefore, we analyzed two protocols to explore whether target-phase influences ERNA amplitudes: cortical alpha-triggered PLDBS and STN beta-triggered PLDBS. Significant effect of the target-phase on ERNA amplitude was observed in Participant 1 ($F(3, 1690) = 28.53$, $P < 0.0001$, $R = 0.2195$), Participant 2 ($F(3, 1303) = 41.66$, $P < 0.0001$, $R = 0.2195$) and Participant 3 ($F(3, 1221) = 3.742$, $P = 0.0108$, $R = 0.0875$) under cortical alpha-triggered PLDBS, while no significant differences were found in Participants 4 ($F(3, 1910) = 2.42$, $P = 0.085$, $R = 0.059$) as shown in Fig. 6A. Repeated tests on randomly selected subsamples confirmed that the effects were robust in Participant 1 ($P = 0.00586 \pm 0.02763$) and Participant 2 ($P = 1.84 \times 10^{-5} \pm 0.00021$), but not in Participant 3 ($P = 0.42338 \pm 0.28785$) or Participant 4 ($P = 0.4234 \pm 0.2879$). Similarly, unpaired t-tests comparing ERNA amplitudes between rising and falling phases (Fig. 6B) revealed significant differences in Participant 1 ($t(1035) = 4.416$, $P = 0.0007$) and Participant 2 ($t(667) = 5.815$, $P < 0.0001$), but not in Participant 3 ($t(533) = 1.56$, $P = 0.1228$)) or Participant 4 ($t(903) = 0.4396$, $P = 0.6604$)). Repeated tests on randomly selected subsamples confirmed that the effect remained significant for Participant 2 ($P = 0.01507 \pm 0.0378$), but not for other patients (Participant 1: $P = 0.22692 \pm 0.25048$, Participant 3: $P = 0.38244 \pm 0.28702$, or Participant 4: $P = 0.52812 \pm 0.27852$). Conversely, STN beta-triggered PLDBS demonstrated significant effect of the target-phase on ERNA in all participants, as assessed by within-subject unpaired t-tests (Fig. 6C; 1: $t(3964) = 19.69$, $P < 0.0001$; 2: $t(2893) = 9.832$, $P < 0.0001$; 3: $t(2701) = 11.87$, $P < 0.0001$; 4: $t(3113) = 22.53$, $P < 0.0001$.) Repeated tests on randomly selected subsamples further confirmed the robustness of these phase-dependent effects in Participant 1 ($P = 0.0013529 \pm 0.0092313$), Participant 3 ($P = 0.018049 \pm 0.059673$), and Participant 4 ($P = 0.00019653 \pm 0.0024821$), while the effect in Participant 2 lying near the borderline ($P = 0.067642 \pm 0.15241$).

Table 3
Performance evaluation of real-time phase estimation algorithms.

Methods	ZC		NRO		arHT		SSPE		OscillTrack	
	bias	*std*	*bias*	*std*	*bias*	*std*	*bias*	*std*	*bias*	*std*
Cortical Alpha	$6.81^\circ \pm 4.62^\circ$	$18.37^\circ \pm 6.50^\circ$	$\mathbf{3.18^\circ \pm 6.12^\circ}$	$\mathbf{7.02^\circ \pm 1.86^\circ}$	$28.93^\circ \pm 26.25^\circ$	$9.05^\circ \pm 7.34^\circ$	$18.14^\circ \pm 15.84^\circ$	$7.00^\circ \pm 6.93^\circ$	$3.88^\circ \pm 2.52^\circ$	$8.13^\circ \pm 3.69^\circ$
STN Beta	$11.99^\circ \pm 7.00^\circ$	$25.80^\circ \pm 4.91^\circ$	$\mathbf{9.55^\circ \pm 6.12^\circ}$	$20.58^\circ \pm 2.14^\circ$	$15.16^\circ \pm 10.32^\circ$	$22.60^\circ \pm 1.79^\circ$	$15.45^\circ \pm 11.11^\circ$	$\mathbf{19.53^\circ \pm 2.55^\circ}$	$10.78^\circ \pm 6.84^\circ$	$20.53^\circ \pm 2.04^\circ$

3.6. Differential effect of stimulation phase on bradykinesia

In Participant 4, we tested the effect of different stimulation conditions on motor performance during finger-tapping (Fig. 7A, Supp Fig. 6). Six blocks of PLDBS (in the order of *Falling*, *Rising*, *Rising*, *Falling*, *Rising*, *Falling* and 1.25 min for each block) were delivered after 3 min of cDBS, with at least 5 min interval separating cDBS and PLDBS. During cDBS, we observed a significant increase in finger-tapping velocity (Fig. 7B, $t(121) = 3.399, P = 0.0009$) compared to the OFF-stimulation condition, even though its effect on tapping amplitude was not significant (Fig. 7C, $t(128) = 1.230, P = 0.2209$). One-way ANOVA comparing rising phase PLDBS, falling phase PLDBS, and OFF-stimulation conditions revealed a significant effect of stimulation conditions on finger-tapping velocity (Fig. 7B, $F(2, 238) = 3.394$, $P = 0.0352$) and amplitude (Fig. 7C, $F(2, 248) = 3.252$, $P = 0.043$). Post-hoc analyses showed that PLDBS targeting the rising phase lead to slower and smaller tapping movements compared to PLDBS targeting the falling phase (velocity: *mean difference* $= -0.1707$ $P = 0.0268$; amplitude: *mean difference* $= -0.1355, P = 0.0306$). However, neither PLDBS conditions showed significant differences from the OFF condition in either tapping velocity (rising vs OFF: $P = 0.666$; falling vs OFF: $P = 0.381$) or amplitude (rising vs OFF: $P = 0.296$; falling vs OFF: $P = 0.4289$), indicating phase-specific optimization without overall performance enhancement relative to baseline. Interestingly, the stimulation phase that elicited greater movement effects also exhibited larger ERNA amplitudes.

4. Discussion

In this study, we identified NRO for phase estimation combined with Kalman filter for artifact suppression for PLDBS. We established a system implementing these methods leveraging commonly used neurostimulation hardware with a computer-in-the-loop approach, allowing for continuous cycle-by-cycle PLDBS. Our results show that this system can precisely target four distinct phases of cortical alpha oscillations and two distinct phases of STN beta oscillations. Moreover, STN beta-triggered PLDBS revealed phase-dependent effects on ERNA in the STN and motor performance during a finger-tapping task.

4.1. The stability and accuracy of the proposed PLDBS pipeline

The proposed system demonstrates robust phase stimulation capability, enabling precise delivery of four distinct alpha-phase windows (~10 Hz, 81.24%) and two beta-phase windows (18–25 Hz, 92.64%), with $\pm 45^\circ$ tolerance and $\pm 90^\circ$ tolerance, respectively. Several factors influence stimulation *accuracy*. First, stimulation precision is better for PLDBS targeting cortical alpha compared to PLDBS targeting beta. The performance of real-time phase estimation of the proposed methods depends on spectral characteristics of the target oscillation and the recorded signal. The performance is better for oscillations with a narrower peak frequency band and larger amplitude in the power spectra density of the recorded signal. In Participant 3 who had tremor during the recording, we observed a 7 Hz activity in the EEG recordings which merged with the alpha activity (~10 Hz) in PSD. This broadened stimulation error distributions in EEG-triggered PLDBS (Supp Fig. 4) and reduced stimulation accuracy for EEG-based protocols but not for LFP-triggered PLDBS (Supp Fig. 5). Second, amplitude thresholding reduced phase error variability in both alpha-triggered PLDBS and STN-beta-triggered PLDBS though the effect was weaker for beta-PLDBS. Setting an amplitude thresholding can make sure that the stimulation is only delivered when meaningful oscillations are present.

4.2. The flexibility of the PLDBS system

The proposed PLDBS pipeline is flexible and can be easily integrated with different hardware. For instance, it could be effectively implemented using commercially available hardware, such as Neuro Omega

systems [24,43], even without requiring a computer-in-the-loop, instead relying on built-in driver software for real-time recording and stimulation control. Beyond DBS applications, this pipeline could be directly extended to cycle-by-cycle phase-locked transcranial magnetic stimulation (PLTMS), offering an opportunity to investigate the phase-dependent effects of mu-locked PLTMS [18,20,30,77]. Previous findings suggest a more consistent and shorter intertrial interval could strengthen the relationship between the EEG phase and motor-evoked potential amplitude [78]. Therefore, cycle-by-cycle PLTMS may offer more insight into this debate.

4.3. Potential target-phase-sepecific effects of PLDBS on ERNA and motor performance

Our findings revealed that DBS pulses phase-locked to different phases of STN beta changed the amplitude of ERNA (Fig. 6C). Notably, PLDBS targeting the beta phase with larger ERNA amplitude is also associated better motor outcome in the patient in terms of finger-tapping velocity/amplitude (Fig. 7BC). It has been proposed that ERNA is a subcortical neuronal circuit signature of DBS-mediated engagement of the basal ganglia indirect pathway network [54]. ERNA amplitude has been shown to correlate with clinical improvement during STN-DBS [79]. Here we propose that, in future studies, ERNA amplitude can be used to select the optimal target phase for PLDBS, which may be individualized for different patient, to maximize the clinical effect of PLDBS.

4.4. Limitations

While the PLDBS system demonstrates significant potential, several areas require further refinement. First, the computer-in-the-loop architecture with USB connections between different device introduces inherent jitter and delays, limiting stimulation accuracy. Although our current implementation employed trigger precompensation (advance signal delivery) to mitigate fixed delays, residual jitter (~10 ms in dedicated stimulation/recording units) persisted as an irreducible constraint. Transitioning to embedded systems with more predictable and stable processing could enhance artifact detection, phase estimation precision, and overall simulation-aligned accuracy. Implementing integrated hardware platforms (e.g., Neuro Omega systems) may optimize temporal precision by minimizing inter-device communication latencies.

Second, while Kalman filtering provides robust stability, the current threshold-based detection method still allows some artifact contamination, which can negatively impact AR model predictions. Enhanced approaches could combine Kalman filtering with real-time interpolation to improve robustness. Additionally, the artifact duration parameter (9 ms) restricts the maximum frequency range that can be effectively targeted, necessitating more flexible algorithms; the SynchroStim artifact removal method could provide a robust approach to mitigating the problems caused by the stimulation pulse artifacts [80]. Further, the low sampling rates of implantable devices [81] create additional challenges, requiring optimized recording hardware that balances artifact minimization with computational load [80].

Third, comparative algorithm testing for artifact suppression and real-time phase estimation was conducted exclusively in simulations due to constraints in available time with each patient during externalized DBS testing. Consequently, in real-time patient testing, we implemented only the algorithm demonstrating superior performance in simulation. Future studies are needed to directly compare different methods in patients, ideally within real-world settings in chronically implanted individuals.

Lastly, the study's small sample size limits conclusive assessments of the behavioral impact of PLDBS. While the initial results suggest that PLDBS targeting different phases may lead to different motor outcome, its effects at the current setting were weaker than cDBS, and the PLDBS did not change motor performance from baseline OFF condition in the patient tested in this study. Bursts of high frequency pulses delivered at each updated phase may further increase the effect of PLDBS, however, further testing will be required to test the hypothesis and confirm PLDBS's therapeutic potential.

5. Conclusions

In this study, we compared different methods available required for phase-specific neuromodulation including real-time phase estimation and artifact suppression; evaluated different factors contributing to the potential variability of phase-targeting performance; and demonstrated the feasibility of the selected methods (NRO for phase estimation following Kalman filter for artifact suppression) and hardware pipeline for PLDBS in patients.The system effectively targets distinct cortical alpha and STN beta oscillation phases, demonstrating its precision and adaptability. STN beta-triggered stimulation revealed phase-dependent modulation of ERNA amplitudes and finger-tapping performance, suggesting its potential for motor symptom modulation. However, technical refinements are necessary to improve the system further. Transitioning to embedded hardware enabling simultaneous stimulation and faster processing could reduce jitter and delays, improving phase estimation accuracy. These findings underscore PLDBS's clinical potential as a personalized neuromodulation approach.

CRediT authorship contribution statement

Xuanjun Guo: Writing – review & editing, Writing – original draft, Methodology, Investigation, Formal analysis, Data curation. **Alek Pogosyan:** Validation, Methodology, Investigation, Data curation. **Jean Debarros:** Writing – review & editing, Validation, Methodology, Formal analysis. **Shenghong He:** Writing – review & editing, Validation, Data curation. **Laura Wehmeyer:** Writing – review & editing, Validation, Data curation. **Fernando Rodriguez Plazas:** Validation, Data curation. **Karen Wendt:** Methodology, Formal analysis. **Zixiao Yin:** Writing – review & editing, Data curation. **Ahmed Raslan:** Validation, Data curation. **Thomas Hart:** Validation, Data curation. **Francesca Morgante:** Validation, Data curation. **Tim Denison:** Methodology, Formal analysis. **Erlick A. Pereira:** Validation, Data curation. **Keyoumars Ashkan:** Validation, Data curation. **Shouyan Wang:** Validation, Investigation, Funding acquisition. **Huiling Tan:** Writing – review & editing, Writing – original draft, Validation, Methodology, Investigation, Funding acquisition.

Data accessibility

De-identified data from this study will be made accessible on https://data.mrc.ox.ac.uk/mrcbndu/data-sets/search.

Consent for Publication

All authors approved the final manuscript and the submission to this journal.

Declaration of Competing Interest

KW is currently employed by Magstim Ltd. TD has research agreements with Magstim and Medtronic, and is chief engineer of Amber therapeutics. However, this study did not use any material produced by Magstim Ltd or Amber therapeutics.

Acknowledgements

This work was supported by the Medical Research Council (MC_UU_00003/2). X.G. was supported by China Scholarship Council (No. 202306100220). S.W. and X.G. were supported by National Key Research and Development Program of China (No. 2022YFC2405100);

STI 2030—Major Projects(No. 2021ZD0200407); STI 2030—Major Projects (No. 2022ZD0205300); National Key Research and Development Program of China (No.2021YFF1200600). S.H. was supported by the Guarantors of Brain and Royal Society Sino-British Fellowship Trust (IES\R3\213123). We thank all participants for making this study possible.

Appendix A. Supplementary data

Supplementary data to this article can be found online at https://doi.org/10.1016/j.brs.2025.09.002.

References

[1] Soleimani G, et al. Closing the loop between brain and electrical stimulation: towards precision neuromodulation treatments. Transl Psychiatry 2023;13. https://doi.org/10.1038/s41398-023-02565-5. Preprint at.
[2] Kumari LS, Kouzani AZ. Phase-dependent deep brain stimulation: a review. Brain Sci 2021;11. https://doi.org/10.3390/brainsci11040414. Preprint at.
[3] Hussain SJ, et al. Phase-dependent offline enhancement of human motor memory. Brain Stimul 2021;14:873–83.
[4] Gersner R, Kravetz E, Feil J, Pell G, Zangen A. Long-term effects of repetitive transcranial magnetic stimulation on markers for neuroplasticity: differential outcomes in anesthetized and awake animals. J Neurosci 2011;31:7521–6.
[5] Xu M, et al. Cognitive effects following offline high-frequency repetitive transcranial magnetic stimulation (HF-rTMS) in healthy populations: a systematic review and meta-analysis. Neuropsychol Rev 2024;34:250–76. https://doi.org/10.1007/s11065-023-09580-9. Preprint at.
[6] Pillen S, Shulga A, Zrenner C, Ziemann U, Bergmann TO. Repetitive sensorimotor mu-alpha phase-targeted afferent stimulation produces no phase-dependent plasticity related changes in somatosensory evoked potentials or sensory thresholds. PLoS One 2023;18.
[7] Jansen JM, et al. The effect of high-frequency repetitive transcranial magnetic stimulation on emotion processing, reappraisal, and craving in alcohol use disorder patients and healthy controls: a functional magnetic resonance imaging study. Front Psychiatry 2019;10.
[8] Buzsáki G, Draguhn A. Neuronal oscillations in cortical networks. https://www.science.org; 2004.
[9] Buzsáki G, Anastassiou CA, Koch C. The origin of extracellular fields and currents-EEG, ECoG, LFP and spikes. Nat Rev Neurosci 2012;13:407–20. https://doi.org/10.1038/nrn3241. Preprint at.
[10] Petersen PC, Buzsáki G. Cooling of medial septum reveals theta phase lag coordination of hippocampal cell assemblies. Neuron 2020;107:731–744.e3.
[11] Peles O, Werner-Reiss U, Bergman H, Israel Z, Vaadia E. Phase-specific microstimulation differentially modulates beta oscillations and affects behavior. Cell Rep 2020;30:2555–2566.e3.
[12] Fiene M, et al. Phase-specific manipulation of rhythmic brain activity by transcranial alternating current stimulation. Brain Stimul 2020;13:1254–62.
[13] Reis, C. et al. Phase-specific Deep Brain Stimulation revisited: effects of stimulation on postural and kinetic tremor. doi:10.1101/2022.06.16.22276451.
[14] Santostasi G, et al. Phase-locked loop for precisely timed acoustic stimulation during sleep. J Neurosci Methods 2016;259:101–14.
[15] Gordon PC, Belardinelli P, Stenroos M, Ziemann U, Zrenner C. Prefrontal theta phase-dependent rTMS-induced plasticity of cortical and behavioral responses in human cortex. Brain Stimul 2022;15:391–402.
[16] Nieuwhof F, et al. Phase-locked transcranial electrical brain stimulation for tremor suppression in dystonic tremor syndromes. Clin Neurophysiol 2022;140:239–50.
[17] Schilberg L, Oever S Ten, Schuhmann T, Sack AT. Phase and power modulations on the amplitude of TMS-induced motor evoked potentials. PLoS One 2021;16.
[18] Zrenner C, et al. Corticospinal excitability is highest at the early rising phase of sensorimotor μ-rhythm. Neuroimage 2023;266.
[19] Wischnewski M, Haigh ZJ, Shirinpour S, Alekseichuk I, Opitz A. The phase of sensorimotor mu and beta oscillations has the opposite effect on corticospinal excitability. Brain Stimul 2022;15:1093–100.
[20] Torrecillos F, et al. Motor cortex inputs at the optimum phase of beta cortical oscillations undergo more rapid and less variable corticospinal propagation. J Neurosci 2020;40:369–81.
[21] Mansouri F, et al. A real-time phase-locking System for non-invasive brain stimulation. Front Neurosci 2018;12.
[22] Dondé C, et al. The effects of transcranial electrical stimulation of the brain on sleep: a systematic review. Front Psychiatr 2021;12. https://doi.org/10.3389/fpsyt.2021.646569. Preprint at.
[23] Mansouri F, Dunlop K, Giacobbe P, Downar J, Zariffa J. A fast EEG forecasting algorithm for phase-locked transcranial electrical stimulation of the human brain. Front Neurosci 2017;11.
[24] Escobar Sanabria D, et al. Controlling pallidal oscillations in real-time in Parkinson's disease using evoked interference deep brain stimulation (eiDBS): proof of concept in the human. Brain Stimul 2022;15:1111–9.
[25] Escobar Sanabria D, et al. Real-time suppression and amplification of frequency-specific neural activity using stimulation evoked oscillations. Brain Stimul 2020;13:1732–42.
[26] Santostasi G, et al. Phase-locked loop for precisely timed acoustic stimulation during sleep. J Neurosci Methods 2016;259:101–14.
[27] Ngo HVV, Martinetz T, Born J, Mölle M. Auditory closed-loop stimulation of the sleep slow oscillation enhances memory. Neuron 2013;78:545–53.
[28] Neacsiu AD, et al. Enhancing cognitive restructuring With concurrent repetitive transcranial magnetic stimulation: a transdiagnostic randomized controlled trial. 2021. https://doi.org/10.1101/2021.01.18.21250060.
[29] Mansouri F, et al. Effect of theta transcranial alternating Current stimulation and phase-locked transcranial pulsed Current stimulation on learning and cognitive control. Front Neurosci 2019;13.
[30] Bergmann TO, Lieb A, Zrenner C, Ziemann U. Pulsed facilitation of corticospinal excitability by the sensorimotor μ-alpha rhythm. J Neurosci 2019;39:10034–43.
[31] Cagnan H, et al. Phase dependent modulation of tremor amplitude in essential tremor through thalamic stimulation. Brain 2013;136:3062–75.
[32] McNamara CG, Rothwell M, Sharott A. Stable, interactive modulation of neuronal oscillations produced through brain-machine equilibrium. Cell Rep 2022;41.
[33] Holt AB, et al. Phase-dependent suppression of beta oscillations in parkinson's disease patients. J Neurosci 2019;39:1119–34.
[34] Miyauchi E, et al. A novel approach for assessing neuromodulation using phase-locked information measured with TMS-EEG. Sci Rep 2019;9.
[35] Sun, X. et al. Increased entrainment and decreased excitability predict efficacious treatment of closed-loop phase-locked RTMS for treatment-resistant depression.
[36] Peles O, Werner-Reiss U, Bergman H, Israel Z, Vaadia E. Phase-specific microstimulation differentially modulates beta oscillations and affects behavior. Cell Rep 2020;30:2555–2566.e3.
[37] Lio G, Thobois S, Ballanger B, Lau B, Boulinguez P. Removing deep brain stimulation artifacts from the electroencephalogram: issues, recommendations and an open-source toolbox. Clin Neurophysiol 2018;129:2170–85. https://doi.org/10.1016/j.clinph.2018.07.023. Preprint at.
[38] Swann NC, et al. Adaptive deep brain stimulation for Parkinson's disease using motor cortex sensing. J Neural Eng 2018;15.
[39] Quinn EJ, et al. Beta oscillations in freely moving Parkinson's subjects are attenuated during deep brain stimulation. Mov Disord 2015;30:1750–8.
[40] Neumann WJ, Gilron R, Little S, Tinkhauser G. Adaptive deep brain stimulation: from experimental evidence toward practical implementation. Mov Disord 2023;38:937–48. https://doi.org/10.1002/mds.29415. Preprint at.
[41] Qian X, et al. A method for removal of deep brain stimulation artifact from local field potentials. IEEE Trans Neural Syst Rehabil Eng 2017;25:2217–26.
[42] Heffer LF, Fallon JB. A novel stimulus artifact removal technique for high-rate electrical stimulation. J Neurosci Methods 2008;170:277–84.
[43] Nie Y, et al. Real-time removal of stimulation artifacts in closed-loop deep brain stimulation. J Neural Eng 2021;18.
[44] Zhou A, Johnson BC, Muller R. Toward true closed-loop neuromodulation: artifact-free recording during stimulation. Curr Opin Neurobiol 2018;50:119–27. https://doi.org/10.1016/j.conb.2018.01.012. Preprint at.
[45] Boashash B. Estimating and interpreting the instantaneous frequency of a signal-part 2: algorithms and applications. 1992.
[46] Zanos S, Rembado I, Chen D, Fetz EE. Phase-locked stimulation during cortical beta oscillations produces bidirectional synaptic plasticity in awake monkeys. Curr Biol 2018;28:2515–2526.e4.
[47] Rosenblum MG, et al. Locking-based frequency measurement and synchronization of chaotic oscillators with complex dynamics. Phys Rev Lett 2002;89.
[48] Zrenner C, et al. The shaky ground truth of real-time phase estimation. Neuroimage 2020;214.
[49] Schreglmann SR, et al. Non-invasive suppression of essential tremor via phase-locked disruption of its temporal coherence. Nat Commun 2021;12.
[50] Wodeyar A, Schatza M, Widge AS, Eden UT, Kramer MA. A state space modeling approach to real-time phase estimation. 2021. https://doi.org/10.7554/eLife.
[51] Wodeyar A, Marshall FA, Chu CJ, Eden UT, Kramer MA. Different methods to estimate the phase of neural rhythms agree but only during times of low uncertainty. eNeuro 2023;10.
[52] Rosenblum M, Pikovsky A, Kühn AA, Busch JL. Real-time estimation of phase and amplitude with application to neural data. Sci Rep 2021;11.
[53] Wang S, et al. Closed-loop adaptive deep brain stimulation in parkinson's disease: procedures to achieve it and future perspectives. J Parkinsons Dis 2023;13:453–71. https://doi.org/10.3233/JPD-225053. Preprint at.
[54] Steiner LA, et al. Neural signatures of indirect pathway activity during subthalamic stimulation in Parkinson's disease. Nat Commun 2024;15.
[55] Wiest C, et al. Evoked resonant neural activity in subthalamic local field potentials reflects basal ganglia network dynamics. Neurobiol Dis 2023;178.
[56] Wiest C, et al. Local field potential activity dynamics in response to deep brain stimulation of the subthalamic nucleus in Parkinson's disease. Neurobiol Dis 2020;143.
[57] 42nd Annual International Conferences of the IEEE Engineering in Medicine and Biology Society : 'enabling Innovative Technologies for Global Healthcare' : 20-24 July 2020, Montreal, Canada. IEEE; 2020.
[58] Morbidi F, Garulli A, Prattichizzo D, Rizzo C, Rossi S. Application of Kalman filter to remove TMS-induced artifacts from EEG recordings. IEEE Trans Control Syst Technol 2008;16:1360–6.
[59] Morbidi F, et al. Off-line removal of TMS-induced artifacts on human electroencephalography by Kalman filter. J Neurosci Methods 2007;162:293–302.
[60] Hussain SJ, et al. Phase-dependent offline enhancement of human motor memory. Brain Stimul 2021;14:873–83.
[61] Schaworonkow N, Triesch J, Ziemann U, Zrenner C. EEG-triggered TMS reveals stronger brain state-dependent modulation of motor evoked potentials at weaker stimulation intensities. Brain Stimul 2019;12:110–8.

[62] Busch JL, Feldmann LK, Kühn AA, Rosenblum M. Real-time phase and amplitude estimation of neurophysiological signals exploiting a non-resonant oscillator. Exp Neurol 2022;347.
[63] Wiest C, et al. Local field potential activity dynamics in response to deep brain stimulation of the subthalamic nucleus in Parkinson's disease. Neurobiol Dis 2020;143.
[64] Rosenblum M, Pikovsky A, Kühn AA, Busch JL. Real-time estimation of phase and amplitude with application to neural data. Sci Rep 2021;11.
[65] Thies M, Zrenner C, Ziemann U, Bergmann TO. Sensorimotor mu-alpha power is positively related to corticospinal excitability. Brain Stimul 2018;11:1119–22.
[66] Bergmann TO, Lieb A, Zrenner C, Ziemann U. Pulsed facilitation of corticospinal excitability by the sensorimotor μ-alpha rhythm. J Neurosci 2019;39:10034–43.
[67] Little S, Brown P. The functional role of beta oscillations in Parkinson's disease. Parkinsonism Relat Disord 2014;20(Suppl 1).
[68] Reis C, et al. Phase-specific Deep brain stimulation revisited: effects of stimulation on postural and kinetic tremor. Preprint at 2022. https://doi.org/10.1101/2022.06.16.22276451.
[69] Fischer P, et al. Entraining stepping movements of Parkinson's patients to alternating subthalamic nucleus deep brain stimulation. J Neurosci 2020;40:8964–72.
[70] McNamara CG, Rothwell M, Sharott A. Stable, interactive modulation of neuronal oscillations produced through brain-machine equilibrium. Cell Rep 2022;41.
[71] Salimpour Y, Mills KA, Hwang BY, Anderson WS. Phase- targeted stimulation modulates phase-amplitude coupling in the motor cortex of the human brain. Brain Stimul 2022;15:152–63.
[72] Wiest C, et al. Subthalamic nucleus stimulation–induced local field potential changes in dystonia. Mov Disord 2023;38:423–34.
[73] Holt AB, Wilson D, Shinn M, Moehlis J, Netoff TI. Phasic burst stimulation: a closed-loop approach to tuning deep brain stimulation parameters for parkinson's disease. PLoS Comput Biol 2016;12.
[74] Duchet B, Bogacz R. How to design optimal brain stimulation to modulate phase-amplitude coupling? J Neural Eng 2024;21.
[75] Madsen KH, et al. No trace of phase: corticomotor excitability is not tuned by phase of pericentral mu-rhythm. Brain Stimul 2019;12:1261–70.
[76] Fiene M, et al. Phase-specific manipulation of rhythmic brain activity by transcranial alternating current stimulation. Brain Stimul 2020;13:1254–62.
[77] Desideri D, Zrenner C, Ziemann U, Belardinelli P. Phase of sensorimotor μ-oscillation modulates cortical responses to transcranial magnetic stimulation of the human motor cortex. J Physiol (Paris) 2019;597:5671–86.
[78] Madsen KH, et al. No trace of phase: corticomotor excitability is not tuned by phase of pericentral mu-rhythm. Brain Stimul 2019;12:1261–70.
[79] Sinclair, N. C. et al. Subthalamic Nucleus deep brain stimulation evokes resonant neural activity. doi:10.1002/ana.
[80] Jean Debarros, Gaignon Lea, He Shenghong, Pogosyan Alek, Benjaber Moaad, Denison Timothy. Artefact-free recording of local field potentials with simultaneous stimulation for closed-loop Deep-. Brain Stimul 2020. https://doi.org/10.1109/EMBC44109.2020.9176665.
[81] Schmidt Stephen L, Afsana H, Chowdhury, Mitchell Kyle T, Peters Jennifer J, Gao Qitong, Lee Hui-Jie, Genty Katherine, Chow Shein-Chung, Grill Warren M, Pajic Miroslav, Turner Dennis A. At home adaptive dual target deep brain stimulation in Parkinson's disease with proportional control. Brain 2024;147:749–51.